THEMIS-SHP1 Recruitment by 4-1BB Tunes LCK-Mediated Priming of Chimeric Antigen Receptor-Redirected T Cells

Chuang Sun,[1,5] Peishun Shou,[1,2,5] Hongwei Du,[1] Koichi Hirabayashi,[1] Yuhui Chen,[1] Laura E. Herring,[3] Sarah Ahn,[1,2] Yang Xu,[1] Kyogo Suzuki,[1] Guangming Li,[1] Ourania Tsahouridis,[1] Lishan Su,[1,2] Barbara Savoldo,[1,2,4] and Gianpietro Dotti[1,2,6,*]

[1]Lineberger Comprehensive Cancer Center, University of North Carolina at Chapel Hill, Chapel Hill, NC, USA
[2]Department of Microbiology and Immunology, University of North Carolina at Chapel Hill, Chapel Hill, NC, USA
[3]Michael Hooker Proteomics Center, Department of Pharmacology, University of North Carolina at Chapel Hill, Chapel Hill, NC, USA
[4]Department of Pediatrics, University of North Carolina at Chapel Hill, Chapel Hill, NC, USA
[5]These authors contributed equally
[6]Lead Contact
*Correspondence: gdotti@med.unc.edu
https://doi.org/10.1016/j.ccell.2019.12.014

SUMMARY

Chimeric antigen receptor (CAR) T cell costimulation mediated by CD28 and 4-1BB is essential for CAR-T cell-induced tumor regression. However, CD28 and 4-1BB differentially modulate kinetics, metabolism and persistence of CAR-T cells, and the mechanisms governing these differences are not fully understood. We found that LCK recruited into the synapse of CD28-encoding CAR by co-receptors causes antigen-independent CAR-CD3ζ phosphorylation and increased antigen-dependent T cell activation. In contrast, the synapse formed by 4-1BB-encoding CAR recruits the THEMIS-SHP1 phosphatase complex that attenuates CAR-CD3ζ phosphorylation. We further demonstrated that the CAR synapse can be engineered to recruit either LCK to enhance the kinetics of tumor killing of 4-1BB CAR-T cells or SHP1 to tune down cytokine release of CD28 CAR-T cells.

INTRODUCTION

Chimeric antigen receptors (CARs) are synthetic molecules composed of a single-chain variable fragment (scFv), costimulatory moieties (either CD28 or 4-1BB), and a CD3ζ signaling domain that, when expressed by T lymphocytes, trigger their lytic machinery and costimulation upon antigen engagement (Dotti et al., 2014; Finney et al., 1998; Gross et al., 1989; Imai et al., 2004; Sadelain et al., 2013). In clinical studies, CAR costimulation plays an essential role in promoting the expansion of CAR-redirected T cells, and both CD28 and 4-1BB lead to equally significant clinical responses in B cell malignancies (Brentjens et al., 2013; Maude et al., 2014; Savoldo et al., 2011). However, CD28- and 4-1BB-mediated costimulation in CAR-T cells has been associated with distinct antitumor kinetics because the CD28 endodomain promotes faster antitumor activity compared with the 4-1BB endodomain (Zhao et al., 2015). This phenomenon correlates with the observed pronounced glycolytic metabolism and higher susceptibility to exhaustion of the CD28-mediated costimulation as opposed to the predominantly oxidative metabolism and lower susceptibility to exhaustion of the 4-1BB-mediated costimulation (Kawalekar et al., 2016; Long et al., 2015).

Phosphatidylinositol-4,5-bisphosphate 3-kinase (PI3K) and tumor necrosis factor receptor-associated factors (TRAFs) are known downstream signaling molecules recruited by CD28 and 4-1BB, respectively (Arch and Thompson, 1998; Frauwirth et al., 2002). However, PI3K and TRAF signaling do not explain the observed functional differences between CD28 and 4-1BB costimulation and it remains elusive whether key signaling events occur within the CAR synapse causing the observed kinetics of antitumor activity. Here, we

Significance

Costimulation mediated by CD28 and 4-1BB endodomains integrated into CAR molecules is critical for their antitumor activity. In this study, we have identified that LCK and THEMIS-SHP1 complex are differentially recruited by CD28 and 4-1BB, respectively. Based on these mechanistic findings, we have developed strategies to engineer either LCK or SHP1 in CAR-T cells to specifically tune their functions.

investigated the molecular mechanisms underlying the functional differences between CD28 and 4-1BB costimulation to identify strategies for generating CAR-T cells with more predictable activity and safer clinical profiles.

RESULTS

CD28 Costimulation Promotes Higher Activation of CAR-T Cells via LCK-Mediated Constitutive Phosphorylation of the CAR-CD3ζ Domain

To stringently compare the CD28 and 4-1BB proximal signaling in CAR-T cells, we generated two CARs that encode the same CD19-specific scFv and CD8α stalk, and either the CD28 or the 4-1BB intracytoplasmic costimulatory domain followed by the intracytoplasmic tail of the CD3ζ chain (CAR19.28ζ and CAR19.BBζ) (Figure S1A). Upon activation, transduction and expansion of CAR-T cells for 10–14 days after clinically validated standard operating procedures (Ramos et al., 2016), the magnitude of CAR19.28ζ-T and CAR19.BBζ-T cell activation was measured by stimulating them with titrated doses of an anti-idiotype Ab (α-CAR19 Ab) that crosslinks the CAR (Diaconu et al., 2017). CAR19.28ζ-T cells showed a significantly higher magnitude of activation than CAR19.BBζ-T cells as measured by Ca^{2+} influx (Figure 1A) and higher expression of the early T cell activation marker CD69 in both $CD4^+$ and $CD8^+$ T cells (Figure 1B). Accordingly, CAR19.28ζ-T cells released more interferon γ (IFN-γ) than CAR19.BBζ-T cells (Figure 1C). In contrast, no significant differences in the expression of activation markers and cytokine release were observed when CAR19.28ζ-T and CAR19.BBζ-T cells were stimulated via T cell receptor (TCR) crosslinking (Figure S1B), indicating that the costimulation associated with the CAR determines the magnitude of activation upon CAR engagement. Similar results were obtained when CAR19.28ζ-T and CAR19.BBζ-T cells were simulated via titration of tumor cells expressing the target antigen (Figures 1D and S1C). To confirm our results *in vivo*, CAR19.28ζ-T and CAR19.BBζ-T cells were differentially labeled and infused simultaneously in NSG (NOD-scid $IL2Rg^{null}$) mice bearing $CD19^+$ tumor cells. T cells were then harvested 6 h after infusion. Tumor cells ($CD45^+CD3^-$) and T cells ($CD45^+CD3^+$) were detected in the peripheral blood, bone marrow, lung, and spleen by flow cytometry (Figure 1E). Gating on $CD45^+CD3^+$ T cells and differentially labeled cells, CAR19.28ζ-T cells showed higher expression of CD69 than CAR19.BBζ-T cells in organs that contained less tumor cells, such as blood, lung, and spleen (Figures 1F and S1D–S1F). The stronger activation of CAR19.28ζ-T cells translated into a more pronounced short-term antitumor activity as compared with CAR19.BBζ-T cells when low doses of CAR-T cells were used (Figure S1G).

Proximal signaling molecules are rapidly phosphorylated upon TCR activation in T cells (Smith-Garvin et al., 2009). We observed that CAR19.28ζ-T cells exhibited higher phosphorylation of the downstream proximal signaling molecules CAR-CD3ζ, ZAP70, and LAT when stimulated with the α-CAR19 Ab as compared with CAR19.BBζ-T cells (Figure 1G), and CAR19.28ζ-T cells consistently showed higher antigen-independent/basal phosphorylation of the CAR-CD3ζ (Figures 1H and S1H; Table S1). The latter effect was observed with two other CARs encoding the CD28 endodomain (Figures S1I and S1J), and regardless of the type of hinge or transmembrane domain used within the CAR19 constructs (Figures S1K–S1N). Furthermore, both $CD4^+$ and $CD8^+$ T cells (Figure S1O and S1P) growing with different cytokine(s) (Figures S1Q and S1R) showed higher basal phosphorylation of CAR-CD3ζ in CAR encoding the CD28 endodomain.

LCK kinase confers more profound phosphorylation events in CAR19.28ζ-T cells as compared with CAR19.BBζ-T cells (Salter et al., 2018). We observed that the CAR-CD3ζ basal phosphorylation of CAR19.28ζ-T cells was abrogated by the addition of Src family kinase (PP2) or LCK inhibitor (Inh-II) (Awale and Mohan, 2008) (Figure 2A). Furthermore, pretreatment of CAR19-28ζ-T cells with PP2, which significantly decreases CAR-CD3ζ basal phosphorylation, reduced their responsiveness to CAR crosslinking with low doses of α-CAR19 Ab to similar levels of CAR19.BBζ-T cells, as shown by the expression of CD69 and release of IFN-γ and interleukin-2 (IL-2) (Figures 2B, C, and S2A). In contrast, high doses of α-CAR19 Ab partially overcame the PP2-mediated inhibition in CAR19.28ζ-T cells (Figures 2B, 2C, and S2B). This suggests that LCK is rapidly recruited in the CAR19.28ζ synapse and that a strong CAR aggregation mediated by high doses of α-CAR19 Ab rapidly overcomes the inhibitory effects of PP2 pretreatment. Collectively, these data suggest that higher CAR-CD3ζ basal phosphorylation primes CAR19.28ζ-T cells to a higher magnitude of activity in response to low antigen stimulation.

Co-receptors Recruits LCK within the CAR Synapse

LCK binds to the PYAPP motif of CD28 (Dobbins et al., 2016; Hofinger and Sticht, 2005; Holdorf et al., 1999). However, we observed that introduction of loss-of-function mutations to the PYAPP motif of CAR19.28ζ (CAR19.28AAAζ, CAR19.28YFζ, or CAR19.28AFAAζ) (Figures 3A and 3B) did not completely abolish the association of LCK to CAR19.28ζ (Figure S3A). Similarly, basal CAR-CD3ζ phosphorylation was only modestly reduced (Figures S3B and S3C), and the cytokine production of CAR19.28ζ-T cells remained unaffected (Figure 3C). Since no significant differences were observed between CD28 mutants and CAR19.28ζ in both phosphorylation of the CAR-CD3ζ and cytokine production, we chose one representative mutant to monitor CD69 expression after α-CAR19 activation. There were no significant differences on CD69 level between CAR19.28ζ and CAR19.28AAAζ mutation either upon CAR or TCR crosslinking (Figures S3D and S3E). Furthermore, in CAR molecules pulled down from CAR.19.BBζ-T cells we observed the presence of LCK (Figure 3D) even if the human 4-1BB endodomain does not contain any known LCK binding motifs (Kim et al., 1993; Wen et al., 2002). These observations suggest that LCK is recruited to the CAR synapse by co-receptors rather than by the CAR-associated CD28 moiety (Rudd et al., 1988; Veillette et al., 1988). By co-immunoprecipitation-mass spectrometry (coIP-MS), we detected unique CD8α peptides spanning regions absent in the CAR-CD8α stalk in CARs pulled down from both CAR19.28ζ-T and CAR.19.BBζ-T cells (Table S2). Furthermore, overexpression of a CD8α mutant that cannot bind to LCK (CD8α-SKS, CKCP mutated to SKSP) (Turner et al., 1990) greatly reduced the basal CAR-CD3ζ phosphorylation in $CD4^+$ T cells expressing the CAR19.28ζ, while $CD4^+$ T cells co-expressing CAR.19.BBζ and the wild-type

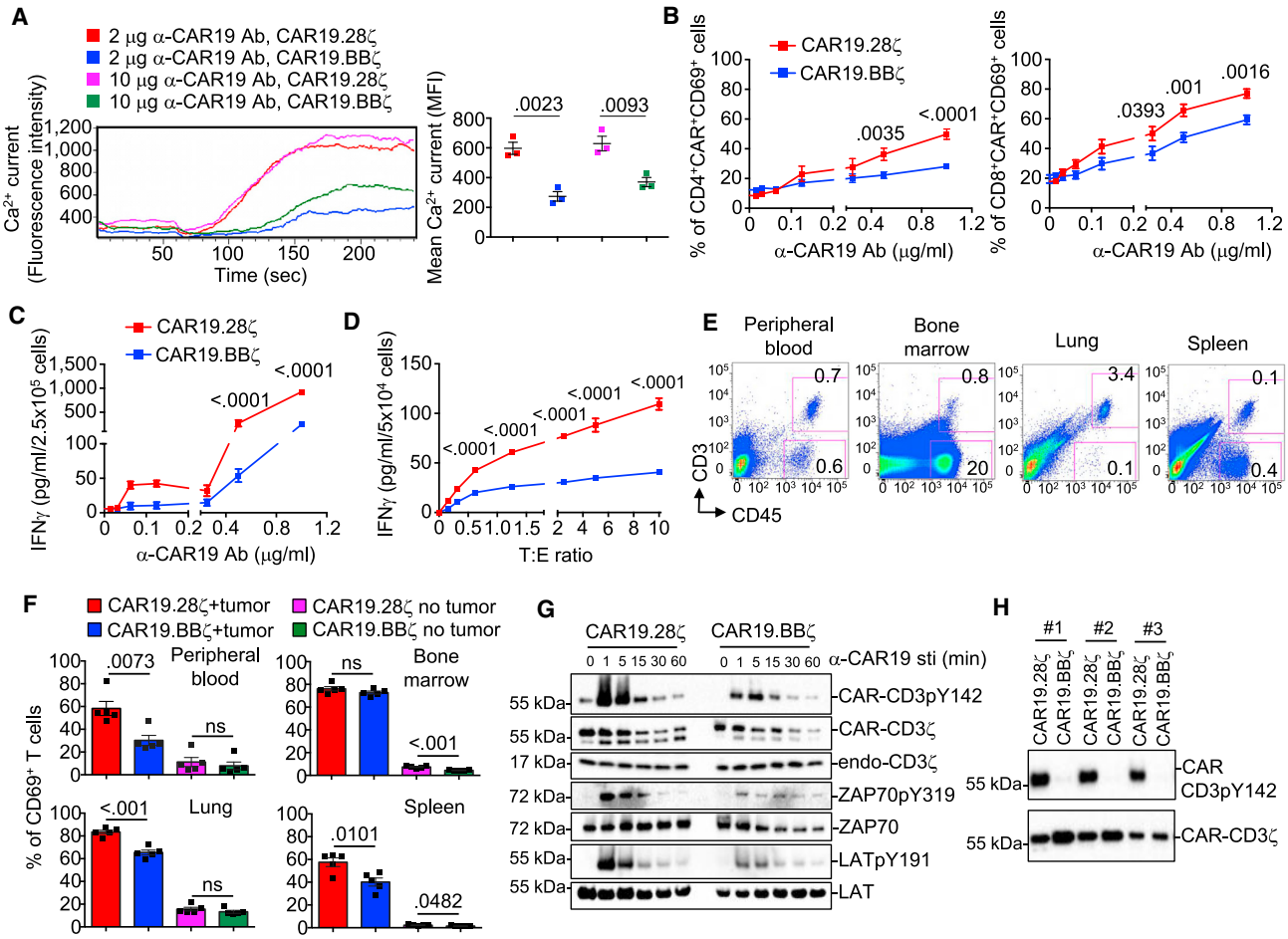

Figure 1. CAR19.28ζ-T Cells Show Higher Magnitude of Activation than CAR19.BBζ-T Cells after CAR Crosslinking

(A–C) CAR19.28ζ-T and CAR19.BBζ-T cells were stimulated with different concentrations of α-CAR19 Ab and Ca^{2+} influx (A), CD69 expression in $CD4^+$ and $CD8^+$ T cells (B), and IFN-γ release (C) were measured: n = 3 in (A), one-way ANOVA; n = 17 in (B), n = 3 in (C), two-way ANOVA.

(D) CAR19.28ζ-T and CAR19.BBζ-T cells were stimulated with the $CD19^+$ BV173 cell line at different tumor to T cell ratios (T:E). IFN-γ levels in the culture supernatants were measured (n = 4, two-way ANOVA).

(E and F) NSG mice engrafted with the $CD19^+$ Daudi cell line were infused with differentially labeled CAR19.28ζ-T and CAR19.BBζ-T cells mixed at a 1:1 ratio. Samples were collected 6 h after infusion. Non-tumor-bearing NSG mice, infused with mixed CAR19.28ζ-T and CAR19.BBζ-T cells, were used as a negative control. Representative flow cytometry plots showing T cells ($CD45^+CD3^+$) and Daudi tumor cells ($CD45^+CD3^-$) identified in the peripheral blood, bone marrow, lung, and spleen (E). Summary of CD69 expression in T cells (n = 5, two-tailed unpaired t test) (F).

(G) Phosphorylation of CAR-CD3ζ, ZAP70, and LAT in CAR19.28ζ-T and CAR19.BBζ-T cells after stimulation with the α-CAR19 Ab at 10 μg/mL. Cells were incubated with the α-CAR19 Ab followed by incubation with a goat anti-mouse IgG secondary antibody on ice. CAR-T cells were then transferred to 37°C for indicated time to be activated (n = 3).

(H) CAR-CD3ζ phosphorylation of CAR19.28ζ-T and CAR.19.BBζ-T cells in the absence of CAR crosslinking. Total CAR detected by the CD3ζ chain Ab was used as equal loading. Results of three representative donors are shown. All data are presented as mean ± SEM.

See also Figure S1 and Table S1.

CD8α (CD8α-WT) showed increased basal CAR-CD3ζ phosphorylation (Figures 3E and S3F). We did not find any peptide of the CD4 co-receptor in the CAR19.28ζ pull-down product in coIP-MS even if $CD4^+$ T cells were still present at days 10–14 of culture. However, overexpression of the wild-type CD4 in both $CD4^+$ and $CD8^+$ CAR19.BBζ-T cells increased the basal phosphorylation of CAR-CD3ζ (Figure 3F). As observed for TCR signaling (Wiest et al., 1996), our data support the conclusion that LCK recruited to the CAR synapse by either CD8 or CD4 co-receptors plays a major role in triggering the basal CAR-CD3ζ phosphorylation.

THEMIS-SHP1 Counteracts the Effect of LCK in the CAR Synapse of CAR-T Cells Encoding 4-1BB

Although co-receptors bring LCK into the CAR19.BBζ synapse (Figures 3D–3F and S3F; Table S2), we observed very low basal phosphorylation of the CAR-CD3ζ, suggesting that 4-1BB may recruit phosphatases to the CAR synapse that counter the LCK-mediated phosphorylation. Indeed, the tyrosine phosphatase inhibitor Na_3VO_4 promoted antigen-independent phosphorylation of CAR-CD3ζ in CAR19.BBζ-T cells (Figure 4A). Accordingly, coIP-MS demonstrated that THEMIS is more abundantly associated with CAR19.BBζ than CAR19.28ζ (Table S2).

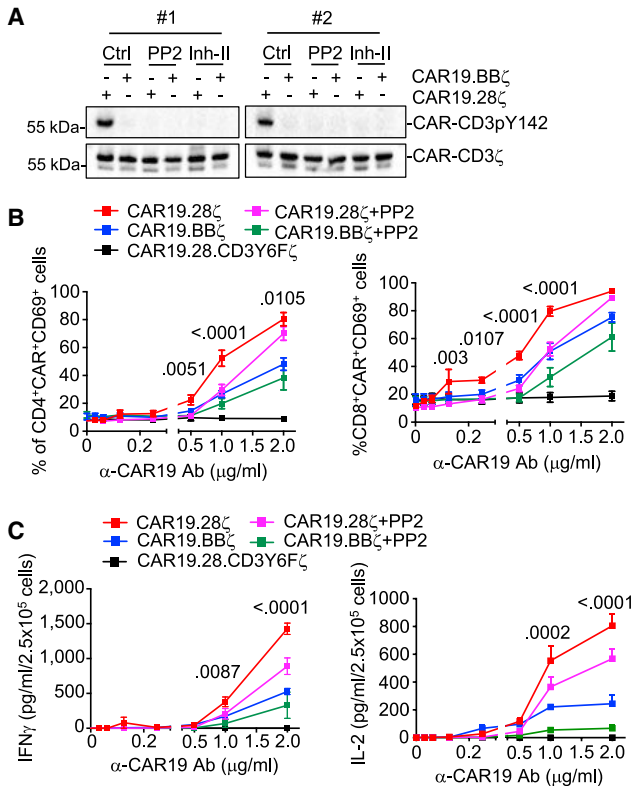

Figure 2. CAR-CD3ζ Basal Phosphorylation Causes Higher Magnitude of Activation of CAR19.28ζ-T Cells than CAR19.BBζ-T Cells after CAR Crosslinking

(A) Phosphorylation of CAR-CD3ζ in CAR19.28ζ-T and CAR19.BBζ-T cells treated with DMSO (Ctrl), Src family kinase (PP2), or LCK (Inh-II) inhibitors at 10 μM for 16 h. Results of two representative donors are shown.

(B) CD69 expression in CAR19.28ζ-T and CAR.19.BBζ-T cells pretreated with 10 μM PP2 for 16 h and then stimulated with α-CAR19 Ab at various concentrations for 6 h. CAR19.28ζ-T and CAR19.BBζ-T cells not exposed to PP2 were used as control. An additional negative control is represented by CAR19.CD3Y6Fζ-T cells, which are T cells expressing the CAR19 in which all six tyrosine (Y) residues of the three immunoreceptor tyrosine-based activation motifs of CAR-CD3ζ were mutated to phenylalanine (F) to completely abrogate tyrosine phosphorylation of the CAR-CD3ζ.

(C) CAR19.28ζ-T and CAR19.BBζ-T cells were treated as in (B). Cytokine release were quantified (n = 3 for cytokine release, n = 5 for CD69 expression, two-way ANOVA; p value between CAR19.28ζ-T and CAR19.28ζ-T cells + PP2 groups).

All data are presented as mean ± SEM. See also Figure S2.

Although THEMIS does not have direct phosphatase activity, it binds to the phosphatase SHP1, and then the THEMIS-SHP1 complex is recruited by LAT to the TCR synapse to regulate T cell activation (Paster et al., 2015). THEMIS pull-down in T cells and Jurkat cells co-expressing THEMIS and CARs confirmed a stronger interaction between THEMIS and CAR19.BBζ than THEMIS and CAR19.28ζ (Figures S4A and S4B). Knockdown of THEMIS or SHP1 in CAR19.BBζ-T cells using small hairpin RNA increased their CAR-CD3ζ basal phosphorylation (Figures 4B, 4C, S4C, and S4D), indicating that the THEMIS-SHP1 complex negatively regulates CAR-CD3ζ phosphorylation of CAR19.BBζ. To map the domain of 4-1BB interacting with THEMIS, we generated 4-1BB mutants and found that the COOH-terminal deletion of 10 amino acids abolishes 4-1BB interaction with THEMIS (Figure 4D, 4E, and S4E), leading to increased CAR-CD3ζ phosphorylation (Figure 4F), Ca^{2+} influx (Figures 4G and S4F), CD69 expression, and IFN-γ release (Figures 4H, S4G, and S4H) by the activated CAR19.BBζ-T cells. These data support the conclusion that the THEMIS-SHP1 complex selectively attenuates CAR-CD3ζ phosphorylation in CAR-T cells expressing 4-1BB.

Engineering LCK Kinase Fine-Tunes the Antitumor Activity of CAR-T Cells Encoding 4-1BB

LCK has access to the CAR19.BBζ synapse, but its kinase activity is limited by the presence of the THEMIS-SHP1 complex. Although the COOH-terminal deletion of 10 amino acids abolishing the 4-1BB interaction with THEMIS promotes the rapid activation of CAR19.BBζ-T cells, this deletion also abrogates the binding to TRAF2, which would compromise 4-1BB signaling (Jang et al., 1998). In contrast, LCK overexpression in CAR19.BBζ-T cells may break the balance of kinases and phosphatases within the CAR synapse and promote basal CAR-CD3ζ phosphorylation (Figure 5A). We found that overexpressed LCK retains its native N-terminal myristoylation and palmitoylation (Resh, 1994), and thus accumulates in the cell membrane of CAR19.BBζ-T cells (Figure 5B), increasing the basal phosphorylation of CAR-CD3ζ (Figure 5C) and Ca^{2+} influx upon antigen stimulation (Figures 5D and S5A). CAR19.BBζ-T cells co-expressing LCK expanded numerically *in vivo* in a lymphoma tumor model (Figure 5E), and showed better control of tumor growth at a suboptimal cell dose as compared with CAR19.BBζ-T cells (Figures 5F and S5B). Moreover, CAR19.BBζ-T cells co-expressing LCK better controlled tumor growth after tumor re-challenge as compared with CAR19.28ζ-T cells (Figure 5F). The beneficial effect of LCK overexpression in CAR-T cells encoding 4-1BB was also observed in a neuroblastoma model targeting the GD2 antigen (Figures 5G, 5H, and S5C), without causing any increase in the expression of PD-1 or TIM3 in CAR-T cells (Figure 5I). These data support the conclusion that LCK overexpression in CAR-T cells expressing 4-1BB promotes faster antitumor activity without compromising their intrinsic enhanced persistence.

Engineering SHP1 Phosphatase Fine-Tunes the Effector Function of CAR-T Cells Encoding CD28

CAR-T cells infused in patients with significant leukemia or lymphoma tumor burden cause cytokine release syndrome (CRS) (Lee et al., 2014). While the administration of a monoclonal antibody blocking the IL-6 receptor has been demonstrated to be effective in attenuating the CRS, the implementation of a precise pharmacologic control of CAR-T cells remains highly appealing (Diaconu et al., 2017; Foster et al., 2017; Wu et al., 2015). We modified SHP1 allowing it to be pharmacologically recruited to the CAR synapse via the FKBP-FRB heterodimerization process (Figure 6A and S6A). In response to the heterodimerization small molecule AP21967, FKBP-SHP1 forms heterodimers with CAR19.28ζ.FRB, tunes down CAR-CD3ζ phosphorylation upon antigen binding (Figure 6B), and reduces IFN-γ release by CAR19.28ζ-T cells in a reversible manner without compromising their antitumor activity *in vitro* (Figures 6C, S6B, and S6C). Similarly, in a xenograft lymphoma model

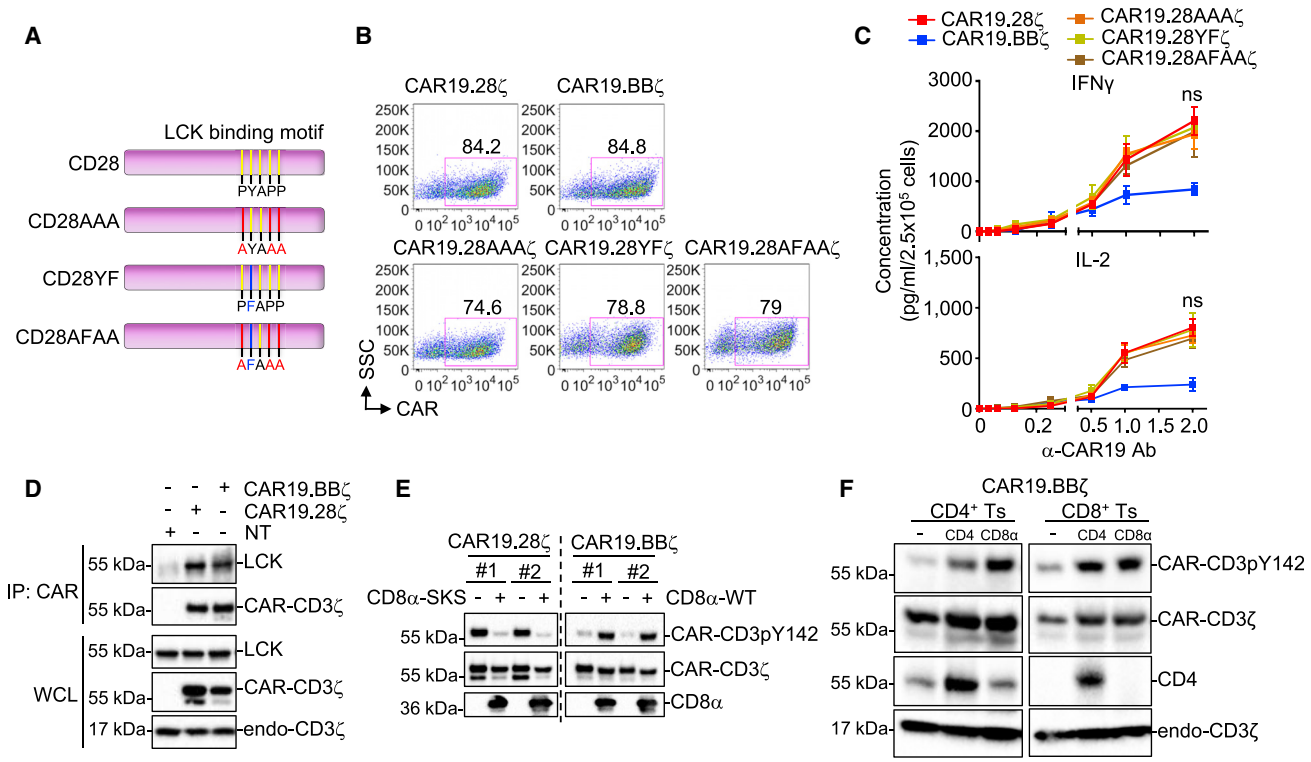

Figure 3. Co-receptors Bring LCK into the CAR Synapse

(A) Schema of the CAR19.28ζ constructs in which specific mutations were included to generate CD28AAA, CD28YF, and CD28AFAA (CD28AAA, mutation of PYAPP to AYAAA; CD28YF, mutation of PYAPP to PFAPP; CD28AFAA, mutation of PYAPP to AFAAA).

(B) Representative flow plots showing the expression of CAR19 in transduced T cells at day 6 of culture.

(C) Cytokine release of CAR-T cells stimulated with the α-CAR19 Ab at different concentrations for 6 h. Cells were collected at day 14 of culture (n = 3, two-way ANOVA; n.s., not significant between CAR19.28ζ-T and CAR19.28AAAζ-T, CAR19.28YFζ-T, or CAR19.28AFAAζ-T cells).

(D) LCK detection by immunoprecipitation (IP) in CAR molecules pulled down from CAR19.28ζ-T and CAR19.BBζ-T cells collected at day 14 of culture.

(E) Phosphorylation of CAR-CD3ζ Y142 in CD4$^+$ T cells expressing either CAR19.28ζ or CAR19.BBζ and co-transduced with the CD8α mutant (CD8α-SKS) or wild-type CD8α (CD8α-WT). Results of two representative donors are shown.

(F) CAR-CD3ζ pY142 phosphorylation in CD4$^+$ or CD8$^+$ CAR19.BBζ-T cells overexpressing either CD4 or CD8α.

All data are presented as mean ± SEM. See also Figure S3 and Table S2.

(Figure 6D), the administration of the AP21967 *in vivo* reduced IFN-γ release by CAR19.28ζ-T cells co-expressing SHP1, without impairing their antitumor effects (Figures 6E and 6F).

Because NSG immunodeficient mice are not appropriate models for CRS we used a humanized mouse model in which CAR-T cell inoculation causes the release of human IL-6 in the plasma of the treated mice (Diaconu et al., 2017; Norelli et al., 2018). This model reconstitutes high amounts of normal human B lymphocytes expressing CD19 that can be targeted by CD19-specific CAR-T cells (Diaconu et al., 2017). In these humanized mice (Figure 6G), SHP1 recruitment induced by the transient administration of AP21967 alleviated their weight loss (Figure 6H) and significantly reduced the release in the plasma of human IFN-γ, IL-6, granulocyte-macrophage colony-stimulating factor, and tumor necrosis factor alpha (Figures 6I and S6D). Importantly, the transient use of AP21967 did not impair the therapeutic effect of CAR19.28ζ-T cells *in vivo* (Figure S6E). The effect of SHP1 heterodimerization *in vivo* on cytokine release was further validated in another CRS model, using SCID-beige mice (Giavridis et al., 2018) (Figures S6F and S6G). Taken together, these data demonstrate that the transient recruitment of SHP1 within the CAR19.28ζ synapse by the heterodimerization small molecule AP21967 can tune down the severity of CRS without impairing the antitumor effects of CAR-T cells.

DISCUSSION

Costimulation plays a fundamental role in promoting the antitumor effects and persistence of CAR-redirected T cells. Here, we demonstrated that CD28 and 4-1BB endodomains incorporated into CAR molecules differentially regulate the equilibrium of phosphorylation and dephosphorylation of the CAR-CD3ζ endodomain and this in turn regulates the magnitude of CAR-T cell activation. Furthermore, we provide data supporting the notion that the equilibrium of LCK/THEMIS-SHP1 can be genetically manipulated to modulated efficacy and safety of CAR-T cells.

It has been recognized in clinical trials that CD19-specific CAR-T cells encoding either CD28 or 4-1BB costimulatory endodomains promote equal antitumor activity in patients with B cell malignancies (Brentjens et al., 2013; Maude

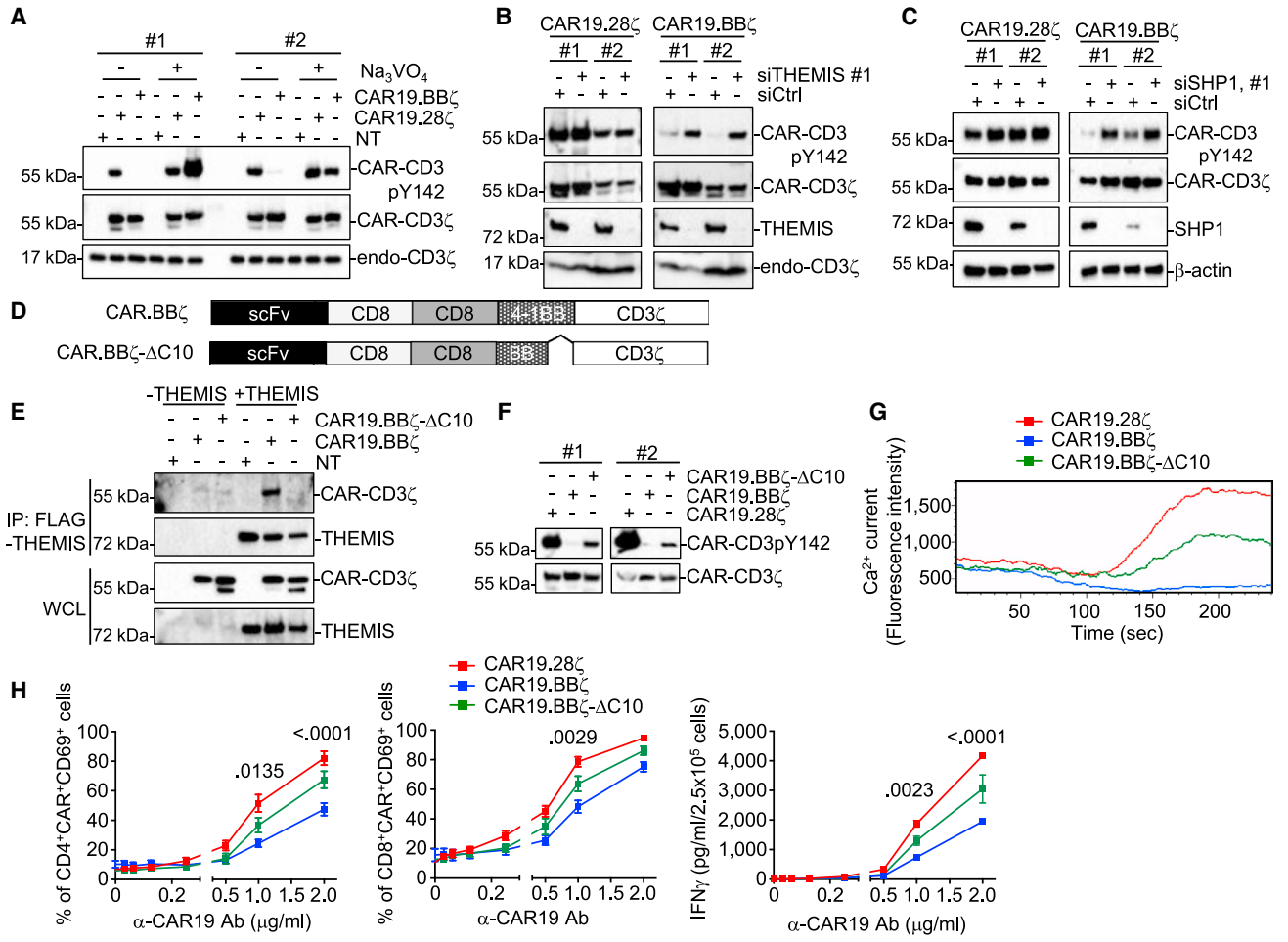

Figure 4. THEMIS-SHP1 Complex Attenuates CAR-CD3ζ Basal Phosphorylation of CAR19.BBζ-T Cells

(A) Phosphorylation of CAR-CD3ζ Y142 in CAR19.28ζ-T and CAR19.BBζ-T cells treated with 200 μM phosphatase inhibitor Na_3VO_4. NT, non-transduced control. Results of two representative donors are shown.

(B) THEMIS expression and CAR-CD3ζ Y142 phosphorylation in CAR19.28ζ-T and CAR19.BBζ-T cells co-transduced with vectors encoding small hairpin RNA (shRNA) specific for THEMIS and selected by puromycin. Results of two representative donors are shown.

(C) CAR19.28ζ-T and CAR19.BBζ-T cells were co-transduced with vectors encoding shRNA specific for SHP1 and selected by puromycin. CAR-CD3ζ Y142 phosphorylation and SHP1 were measured by western blot. Results of two representative donors are shown.

(D) Structures of CAR19.BBζ and its mutant CAR19.BBζ-ΔC10 (deletion of 10 amino acids at the COOH of 4-1BB).

(E) CAR19.BBζ-T or CAR19.BBζ-ΔC10-T cells were co-transduced with a vector encoding FLAG-tagged THEMIS. At day 14 of culture, cells were collected and THEMIS was immunoprecipitated by FLAG IP. CAR in the IP product was detected by western blot using the α-CD3ζ Ab.

(F) Phosphorylation of CAR-CD3ζ Y142 in CAR19.BBζ-T and CAR19.BBζ-ΔC10-T cells. Results of two representative donors are shown.

(G) Ca^{2+} influx in CAR19.28ζ-T cells, CAR19.BBζ-T cells, and CAR19.BBζ-ΔC10-T cells after stimulation with the α-CAR19 Ab. Representative of three donors.

(H) CD69 expression and IFN-γ release in CAR19.28ζ-T cells, CAR19.BBζ-T cells, and CAR19.BBζ-ΔC10-T cells upon α-CAR19 Ab stimulation (n = 3 for IFN-γ release, n = 5 for CD69 expression, two-way ANOVA; p value between CAR19.BBζ-T cells and CAR19.BBζ-ΔC10-T cells groups). All data are presented as mean ± SEM. See also Figure S4.

et al., 2014). However, preclinical models showed that CD28 and 4-1BB have fundamental biological differences that may be critical in inducing antitumor effects and in promoting persistence of CAR-T cells. CD28 costimulation is generally associated with a very rapid tumor clearance as compared with 4-1BB, but also more pronounced propensity to exhaustion or less formation of memory T cells as indicated by their short-term persistence (Long et al., 2015; Zhao et al., 2015). Here, we mechanistically link the rapid kinetics of CD28 expressing CAR-T cells with the basal phosphorylation of the CAR-CD3ζ endodomain. The basal phosphorylation is caused by LCK recruited within the CAR synapse, which is largely mediated by co-receptors rather than the CD28 incorporated within the CAR, and imprints CAR-T cells to higher magnitude of response immediately upon encountering the antigen. In sharp contrast, the synapse formed by CAR molecules containing the 4-1BB endodomain selectively recruits the THEMIS-SHP1 complex that dephosphorylates the CAR-CD3ζ endodomain and attenuates T cell activation. We demonstrated a direct interaction between THEMIS and 4-1BB encoded

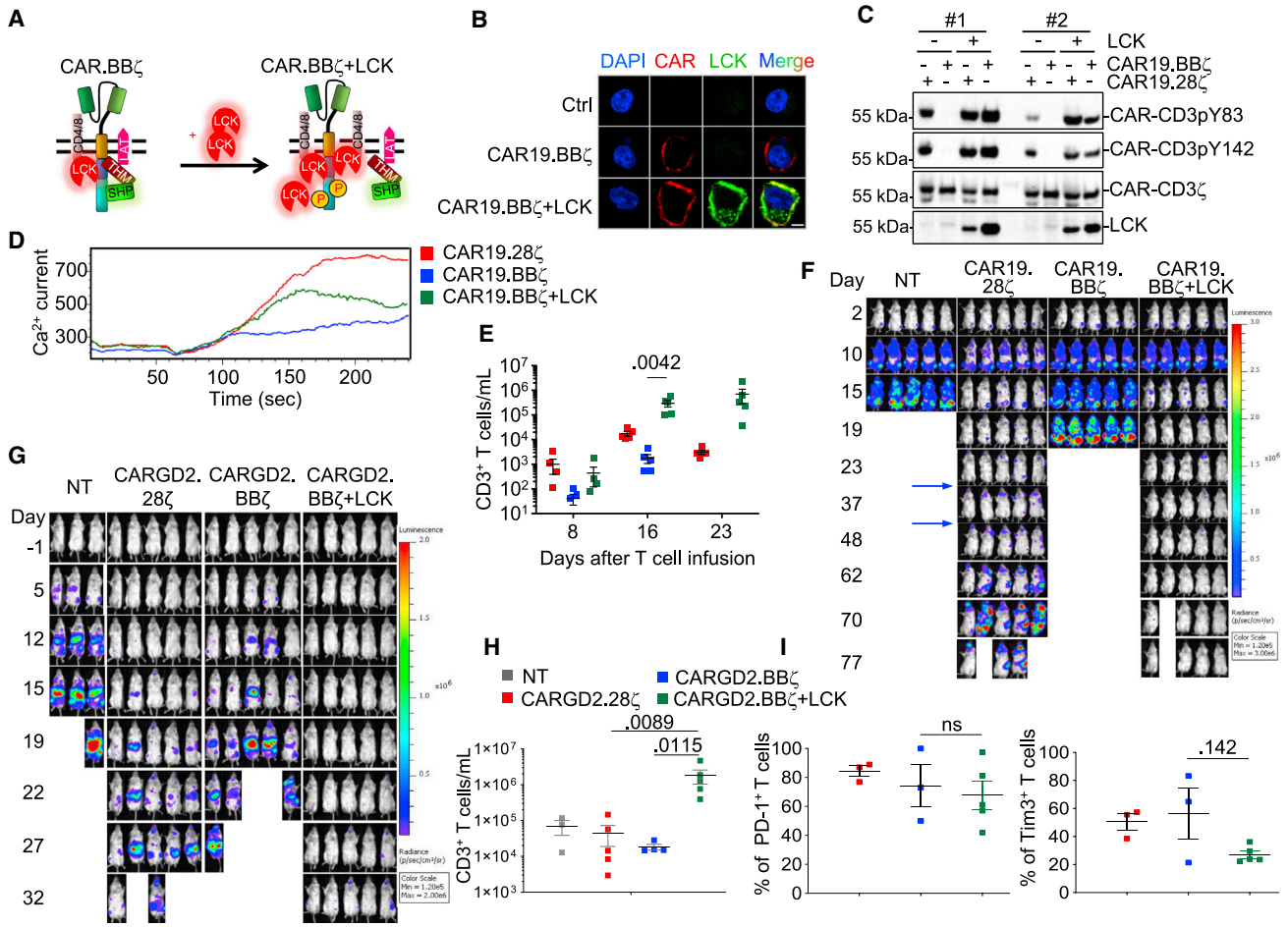

Figure 5. Engineering LCK Kinase in CAR-T Cells Encoding 4-1BB Enhances Their Antitumor Activity *In Vitro* and *In Vivo*

(A) Schema illustrating LCK engineering to counter the phosphatase activity of the THEMIS-SHP1 complex in CAR19.BBζ-T cells.

(B) Confocal microscopy showing the LCK accumulation in the membrane in CAR19.BBζ-T cells co-transduced with the FLAG-tagged LCK. Scale bar, 5 μm. The experiment was replicated in three donors.

(C) Phosphorylation of the CAR-CD3ζ Y83 and Y142 in CAR19.28ζ-T and CAR19.BBζ-T cells expressing LCK. Results of two representative donors are shown.

(D) Representative of Ca^{2+} influx in CAR19.28ζ-T cells and CAR19.BBζ-T cells with or without co-expression of LCK.

(E and F) Quantification of T cells in the peripheral blood (E) and tumor growth monitored by bioluminescence imaging (BLI) (F) in NSG mice engrafted with the $CD19^+$ Daudi cells and infused with CAR19.28ζ-T cells or CAR19.BBζ-T cells with or without LCK. Re-challenging with Daudi cells was performed at days 25 and 40 after initial CAR-T cell infusion (indicated by arrows) (n = 5, one-way ANOVA).

(G) Tumor growth monitored by BLI in NSG mice engrafted with the neuroblastoma tumor cell line CHLA-255 and infused with either CARGD2.28ζ-T or CARGD2.BBζ-T cells with or without LCK.

(H and I) T cell number at day 18 (H), and expression of PD-1 and TIM3 at day 22 (I) in circulating CAR-T cells in mice engrafted with the neuroblastoma tumor cells and treated as described in (G) (n = 3 in NT group, n = 5 in other groups, one-way ANOVA).

All data are presented as mean ± SEM. See also Figure S5.

within the CAR by overexpressing a tagged THEMIS, while we were not able to show the direct interaction with the endogenous THEMIS. We attribute this weakness to the lack of appropriate reagents to immune precipitate the endogenous THEMIS. However, all performed experiments highlight the biological relevance of the discovered interaction between THEMIS and 4-1BB in CAR molecules.

Our mechanistic discoveries have immediate translational implications because kinases and phosphatases can be engineered in CAR-T cells to either enhance or tune down their activation. We demonstrated that LCK, when overexpressed in CAR19.BBζ-T cells, breaks the balance of kinases and phosphatases within the CAR synapse increasing the basal phosphorylation of CAR-CD3ζ and the speed of their antitumor effects. However, while CD28 costimulated CAR-T cells are prone to rapid contraction and possible exhaustion, LCK overexpression in 4-1BB costimulated CAR-T cells does not affect the intrinsic property of 4-1BB signaling to promote T cell persistence since the antitumor response is maintained after tumor re-challenge. Enhancing the kinetics of antitumor activity of 4-1BB, while preserving their longevity, may be critical in controlling rapidly progressive solid tumors.

Toxicities associated with CAR-T cells, such as CRS, remain of concern (Lichtman and Dotti, 2017). Pharmacologic and

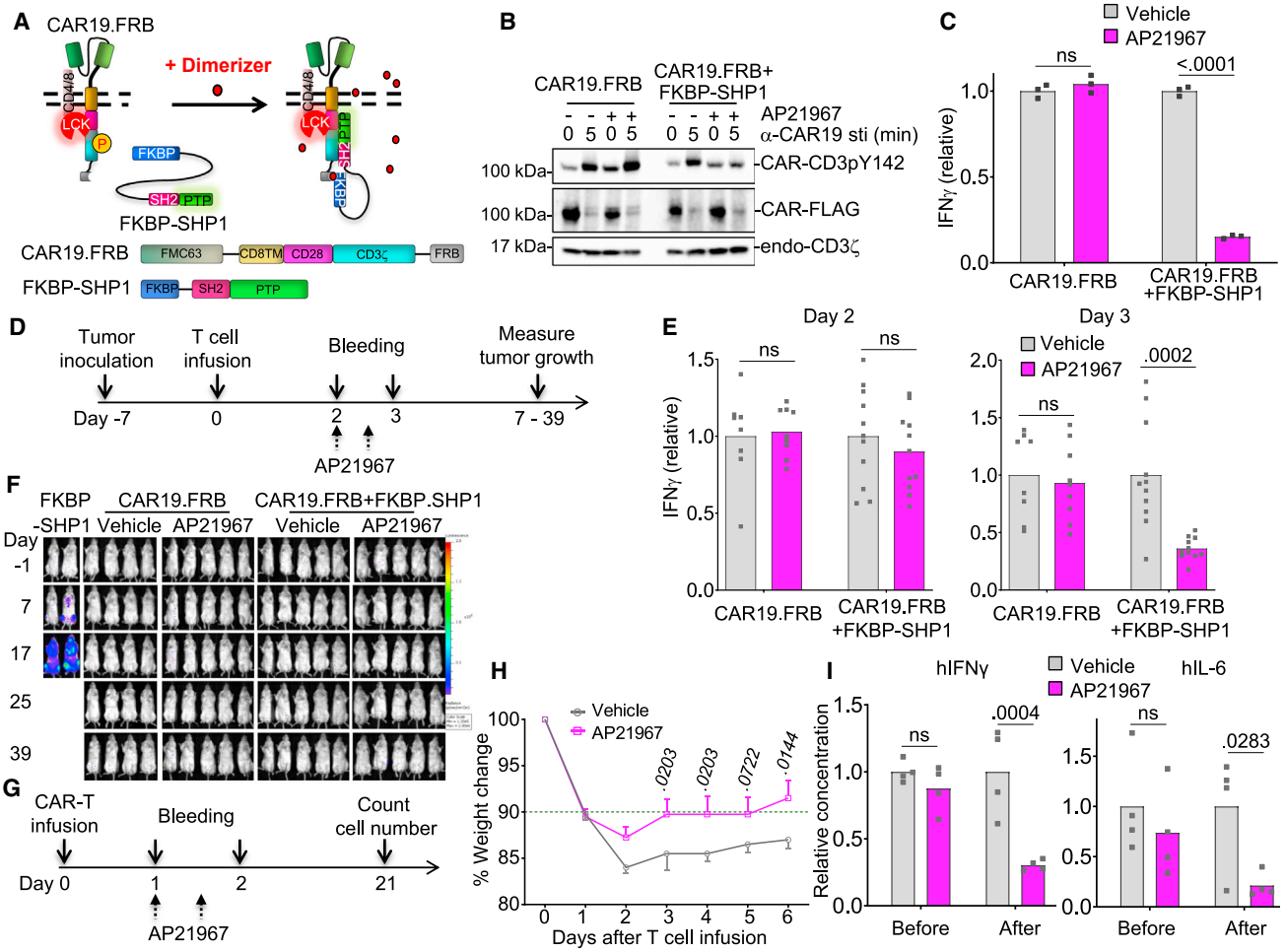

Figure 6. Engineering SHP1 Phosphatase in CAR-T Cells Encoding CD28 Ameliorates Cytokine Release Syndrome

(A) Schema of the FRB and FKBP domain engineering of SHP1 and CARs to pharmacologically control SHP1 recruitment to the CAR19.28ζ synapse.

(B) Phosphorylation of CAR-CD3ζ pY142 in CAR19.28ζ.FRB-T cells alone or co-transduced with FKBP-SHP1 after the stimulation with α-CAR19 Ab in the presence of vehicle (ethanol) or 1 μM AP21967. The experiment was replicated in three donors.

(C) IFN-γ release in the supernatant by CAR19.28ζ.FRB-T cells alone or co-transduced with FKBP-SHP1 and incubated with the $CD19^+$ BV173 tumor cell line at a 1:5 ratio in the presence of vehicle or AP21967 (n = 3, values were normalized to average values in vehicle groups, two-way ANOVA; representative of three donors).

(D) Schema of the NSG mouse model to evaluate the effects of SHP1 heterodimerization in CAR-T cells *in vivo*. Plasma was collected at days 2 and 3 after T cell infusion. AP21967 was administrated twice at day 2 every 12 h.

(E) IFN-γ level in the plasma of mice illustrated in (D) before (day 2) and after (day 3) the administration of vehicle or AP21967 (n = 9–11, values were normalized to average values in vehicle groups, two-way ANOVA; pooled data from two independent experiments).

(F) Representative tumor growth monitored by BLI in NSG mice described as in (D) (n = 4–5, representative of two independent experiments).

(G) Schema of the humanized mouse model to evaluate the effects of SHP1 heterodimerization in CAR-T cells *in vivo*. Plasma was collected at days 1 and 2 after the infusion of CAR-T cells targeting CD19 and co-expressing SHP1. AP21967 was administrated twice at day 1 every 12 h.

(H and I) Weight change (H), and cytokine detection (I) in humanized mice illustrated in (G) after CAR-T cell infusion. Weight was normalized to the starting weight before CAR-T cell infusion. Human IFN-γ and IL-6 were detected before (day 1) and after (day 2) the administration of vehicle or AP21967 (n = 4, two-way ANOVA). All data are presented as mean ± SEM. See also Figure S6.

remote control of CAR-T cells has been explored to modulate CAR-T cell expansion *in vivo* and mitigate side effects (Diaconu et al., 2017; Foster et al., 2017; Wu et al., 2015). While the remote control of T cell proliferation remains challenging in the clinical setting, our mechanistic observation suggests that a temporary break of T cell activation can be achieved via phosphatase engineering. Phosphatases play a critical role in attenuating CAR signaling and we demonstrated that SHP1 can be pharmacologically recruited to the CAR synapse and temporarily attenuate T cell function without eliminating CAR-T cells.

In summary, CD28 and 4-1BB differentially regulate the equilibrium of phosphorylation and dephosphorylation of the CAR-CD3ζ, which in turn regulates the magnitude of CAR-T cell activation. Engineering kinases and phosphatases can be used to tune CAR-T cell function for adoptive immunotherapy.

STAR★METHODS

Detailed methods are provided in the online version of this paper and include the following:

- KEY RESOURCES TABLE
- LEAD CONTACT AND MATERIALS AVAILABILITY
- EXPERIMENTAL MODEL AND SUBJECT DETAILS
  - Cell Lines and Cell Culture
  - Human Samples
  - Mouse Studies
- METHOD DETAILS
  - Plasmids
  - Retrovirus and Lentivirus Production
  - Transduction and Expansion of Human T Cells
  - Flow Cytometry and Cell Phenotyping
  - Activation of CD19-Specific CAR-T Cells with the Anti-idiotype Ab or $CD19^+$ Tumor Cells
  - Cytokine Measurements
  - Ca^{2+} Influx Assay
  - Immunoprecipitation (IP)
  - Western Blot
  - Mass Spectrometry
  - Xenograft Mouse Models
  - Cytokine Release Syndrome Models
  - Co-culture Assays
  - Immunofluorescence and Confocal Microscopy
- QUANTIFICATION AND STATISTICAL ANALYSIS
- DATA AND CODE AVAILABILITY

SUPPLEMENTAL INFORMATION

Supplemental Information can be found online at https://doi.org/10.1016/j.ccell.2019.12.014.

ACKNOWLEDGMENTS

The UNC Small Animal Imaging Facility at the Biomedical Imaging Research Center, Microscopy Services Laboratory, Flow Cytometry Core Facility, and Michael Hooker Proteomics Core Facility are supported in part by an NCI Cancer Center Core Support Grant to the UNC Lineberger Comprehensive Cancer Center (P30-CA016086). This work was supported in part by R01-CA193140 from National Cancer Institute, United States (to G.D.); R01-AI136990 from National Institute of Allergy and Infectious Diseases, United States (to L.S.). H.D. is supported by W81XWH-18-1-0441 from Department of Defense, United States.

AUTHOR CONTRIBUTIONS

Conceptualization, C.S., P.S., H.D., K.H., Y.C., S.A., L.E.H., Y.X., B.S., and G.D.; Methodology, C.S., P.S., H.D., K.H., Y.C., S.A., L.E.H., Y.X., K.S., G.L., O.T., L.S., B.S., and G.D.; Investigation, C.S., P.S., H.D., K.H., Y.C., S.A., L.E.H., Y.X., K.S., G.L., O.T., L.S., B.S., and G.D.; Writing – Original Draft, C.S., P.S., and G.D.; Writing – Review & Editing, all authors; Resources, L.E.H.; Supervision, B.S. and G.D.

DECLARATION OF INTERESTS

The engineering processes described in the manuscript have been included in a filed patent application. Dr. Dotti serves in the SAB of Bellicum Pharmaceutical s.p.a. and MolMed s.p.a. No potential conflicts of interest were disclosed by the other authors.

Received: March 18, 2019
Revised: October 21, 2019
Accepted: December 26, 2019
Published: January 30, 2020

REFERENCES

Arch, R.H., and Thompson, C.B. (1998). 4-1BB and Ox40 are members of a tumor necrosis factor (TNF)-nerve growth factor receptor subfamily that bind TNF receptor-associated factors and activate nuclear factor kappaB. Mol. Cell. Biol. *18*, 558–565.

Awale, M., and Mohan, C.G. (2008). Molecular docking guided 3D-QSAR CoMFA analysis of N-4-pyrimidinyl-1H-indazol-4-amine inhibitors of leukocyte-specific protein tyrosine kinase. J. Mol. Model. *14*, 937–947.

Brentjens, R.J., Davila, M.L., Riviere, I., Park, J., Wang, X., Cowell, L.G., Bartido, S., Stefanski, J., Taylor, C., Olszewska, M., et al. (2013). CD19-targeted T cells rapidly induce molecular remissions in adults with chemotherapy-refractory acute lymphoblastic leukemia. Sci. Transl. Med. *5*, 177ra38.

Chen, Y., Sun, C., Landoni, E., Metelitsa, L., Dotti, G., and Savoldo, B. (2019). Eradication of neuroblastoma by T cells redirected with an optimized GD2-specific chimeric antigen receptor and interleukin-15. Clin. Cancer Res. https://doi.org/10.1158/1078-0432.CCR-18-1811.

Diaconu, I., Ballard, B., Zhang, M., Chen, Y., West, J., Dotti, G., and Savoldo, B. (2017). Inducible caspase-9 selectively modulates the toxicities of CD19-specific chimeric antigen receptor-modified T cells. Mol. Ther. *25*, 580–592.

Dobbins, J., Gagnon, E., Godec, J., Pyrdol, J., Vignali, D.A., Sharpe, A.H., and Wucherpfennig, K.W. (2016). Binding of the cytoplasmic domain of CD28 to the plasma membrane inhibits Lck recruitment and signaling. Sci. Signal. *9*, ra75.

Dotti, G., Gottschalk, S., Savoldo, B., and Brenner, M.K. (2014). Design and development of therapies using chimeric antigen receptor-expressing T cells. Immunol. Rev. *257*, 107–126.

Finney, H.M., Lawson, A.D., Bebbington, C.R., and Weir, A.N. (1998). Chimeric receptors providing both primary and costimulatory signaling in T cells from a single gene product. J. Immunol. *161*, 2791–2797.

Foster, A.E., Mahendravada, A., Shinners, N.P., Chang, W.C., Crisostomo, J., Lu, A., Khalil, M., Morschl, E., Shaw, J.L., Saha, S., et al. (2017). Regulated expansion and survival of chimeric antigen receptor-modified T cells using small molecule-dependent inducible MyD88/CD40. Mol.Ther. *25*, 2176–2188.

Frauwirth, K.A., Riley, J.L., Harris, M.H., Parry, R.V., Rathmell, J.C., Plas, D.R., Elstrom, R.L., June, C.H., and Thompson, C.B. (2002). The CD28 signaling pathway regulates glucose metabolism. Immunity *16*, 769–777.

Giavridis, T., van der Stegen, S.J.C., Eyquem, J., Hamieh, M., Piersigilli, A., and Sadelain, M. (2018). CAR T cell-induced cytokine release syndrome is mediated by macrophages and abated by IL-1 blockade. Nat. Med. *24*, 731–738.

Gross, G., Gorochov, G., Waks, T., and Eshhar, Z. (1989). Generation of effector T cells expressing chimeric T cell receptor with antibody type-specificity. Transplant. Proc. *21* (1 Pt 1), 127–130.

Hofinger, E., and Sticht, H. (2005). Multiple modes of interaction between Lck and CD28. J. Immunol. *174*, 3839–3840.

Holdorf, A.D., Green, J.M., Levin, S.D., Denny, M.F., Straus, D.B., Link, V., Changelian, P.S., Allen, P.M., and Shaw, A.S. (1999). Proline residues in CD28 and the Src homology (SH)3 domain of Lck are required for T cell costimulation. J. Exp.Med. *190*, 375–384.

Hoyos, V., Savoldo, B., Quintarelli, C., Mahendravada, A., Zhang, M., Vera, J., Heslop, H.E., Rooney, C.M., Brenner, M.K., and Dotti, G. (2010). Engineering CD19-specific T lymphocytes with interleukin-15 and a suicide gene to enhance their anti-lymphoma/leukemia effects and safety. Leukemia *24*, 1160–1170.

Imai, C., Mihara, K., Andreansky, M., Nicholson, I.C., Pui, C.H., Geiger, T.L., and Campana, D. (2004). Chimeric receptors with 4-1BB signaling capacity provoke potent cytotoxicity against acute lymphoblastic leukemia. Leukemia *18*, 676–684.

Jang, I.K., Lee, Z.H., Kim, Y.J., Kim, S.H., and Kwon, B.S. (1998). Human 4-1BB (CD137) signals are mediated by TRAF2 and activate nuclear factor-kappa B. Biochem. Biophys. Res. Commun. *242*, 613–620.

Kawalekar, O.U., O'Connor, R.S., Fraietta, J.A., Guo, L., McGettigan, S.E., Posey, A.D., Jr., Patel, P.R., Guedan, S., Scholler, J., Keith, B., et al. (2016). Distinct signaling of coreceptors regulates specific metabolism pathways and impacts memory development in CAR T cells. Immunity *44*, 380–390.

Kim, Y.J., Pollok, K.E., Zhou, Z., Shaw, A., Bohlen, J.B., Fraser, M., and Kwon, B.S. (1993). Novel T cell antigen 4-1BB associates with the protein tyrosine kinase p56lck1. J. Immunol. *151*, 1255–1262.

Lee, D.W., Gardner, R., Porter, D.L., Louis, C.U., Ahmed, N., Jensen, M., Grupp, S.A., and Mackall, C.L. (2014). Current concepts in the diagnosis and management of cytokine release syndrome. Blood *124*, 188–195.

Li, G., Cheng, M., Nunoya, J., Cheng, L., Guo, H., Yu, H., Liu, Y.J., Su, L., and Zhang, L. (2014). Plasmacytoid dendritic cells suppress HIV-1 replication but contribute to HIV-1 induced immunopathogenesis in humanized mice. PLoS Pathog. *10*, e1004291.

Lichtman, E.I., and Dotti, G. (2017). Chimeric antigen receptor T-cells for B-cell malignancies. Transl. Res. *187*, 59–82.

Long, A.H., Haso, W.M., Shern, J.F., Wanhainen, K.M., Murgai, M., Ingaramo, M., Smith, J.P., Walker, A.J., Kohler, M.E., Venkateshwara, V.R., et al. (2015). 4-1BB costimulation ameliorates T cell exhaustion induced by tonic signaling of chimeric antigen receptors. Nat. Med. *21*, 581–590.

Maude, S.L., Frey, N., Shaw, P.A., Aplenc, R., Barrett, D.M., Bunin, N.J., Chew, A., Gonzalez, V.E., Zheng, Z., Lacey, S.F., et al. (2014). Chimeric antigen receptor T cells for sustained remissions in leukemia. N. Engl. J. Med. *371*, 1507–1517.

Norelli, M., Camisa, B., Barbiera, G., Falcone, L., Purevdorj, A., Genua, M., Sanvito, F., Ponzoni, M., Doglioni, C., Cristofori, P., et al. (2018). Monocyte-derived IL-1 and IL-6 are differentially required for cytokine-release syndrome and neurotoxicity due to CAR T cells. Nat. Med. *24*, 739–748.

Paster, W., Bruger, A.M., Katsch, K., Gregoire, C., Roncagalli, R., Fu, G., Gascoigne, N.R., Nika, K., Cohnen, A., Feller, S.M., et al. (2015). A THEMIS: SHP1 complex promotes T-cell survival. EMBO J. *34*, 393–409.

Ramos, C.A., Savoldo, B., Torrano, V., Ballard, B., Zhang, H., Dakhova, O., Liu, E., Carrum, G., Kamble, R.T., Gee, A.P., et al. (2016). Clinical responses with T lymphocytes targeting malignancy-associated kappa light chains. J. Clin. Invest. *126*, 2588–2596.

Resh, M.D. (1994). Myristylation and palmitylation of Src family members: the fats of the matter. Cell *76*, 411–413.

Rivera, V.M., Berk, L., and Clackson, T. (2012). Dimerizer-mediated regulation of gene expression in vivo. Cold Spring Harb.Protoc. *2012*, 821–824.

Rudd, C.E., Trevillyan, J.M., Dasgupta, J.D., Wong, L.L., and Schlossman, S.F. (1988). The CD4 receptor is complexed in detergent lysates to a protein-tyrosine kinase (pp58) from human T lymphocytes. Proc. Natl. Acad. Sci. U S A *85*, 5190–5194.

Sadelain, M., Brentjens, R., and Riviere, I. (2013). The basic principles of chimeric antigen receptor design. Cancer Discov. *3*, 388–398.

Salter, A.I., Ivey, R.G., Kennedy, J.J., Voillet, V., Rajan, A., Alderman, E.J., Voytovich, U.J., Lin, C., Sommermeyer, D., Liu, L., et al. (2018). Phosphoproteomic analysis of chimeric antigen receptor signaling reveals kinetic and quantitative differences that affect cell function. Sci. Signal. *11*, https://doi.org/10.1126/scisignal.aat6753.

Savoldo, B., Ramos, C.A., Liu, E., Mims, M.P., Keating, M.J., Carrum, G., Kamble, R.T., Bollard, C.M., Gee, A.P., Mei, Z., et al. (2011). CD28 costimulation improves expansion and persistence of chimeric antigen receptor-modified T cells in lymphoma patients. J. Clin. Invest. *121*, 1822–1826.

Smith-Garvin, J.E., Koretzky, G.A., and Jordan, M.S. (2009). T cell activation. Annu. Rev. Immunol. *27*, 591–619.

Sun, C., Mahendravada, A., Ballard, B., Kale, B., Ramos, C., West, J., Maguire, T., McKay, K., Lichtman, E., Tuchman, S., et al. (2019). Safety and efficacy of targeting CD138 with a chimeric antigen receptor for the treatment of multiple myeloma. Oncotarget. *10*, 2369–2383.

Turner, J.M., Brodsky, M.H., Irving, B.A., Levin, S.D., Perlmutter, R.M., and Littman, D.R. (1990). Interaction of the unique N-terminal region of tyrosine kinase p56lck with cytoplasmic domains of CD4 and CD8 is mediated by cysteine motifs. Cell *60*, 755–765.

Veillette, A., Bookman, M.A., Horak, E.M., and Bolen, J.B. (1988). The CD4 and CD8 T cell surface antigens are associated with the internal membrane tyrosine-protein kinase p56lck. Cell *55*, 301–308.

Vera, J., Savoldo, B., Vigouroux, S., Biagi, E., Pule, M., Rossig, C., Wu, J., Heslop, H.E., Rooney, C.M., Brenner, M.K., and Dotti, G. (2006). T lymphocytes redirected against the kappa light chain of human immunoglobulin efficiently kill mature B lymphocyte-derived malignant cells. Blood *108*, 3890–3897.

Wen, T., Bukczynski, J., and Watts, T.H. (2002). 4-1BB ligand-mediated costimulation of human T cells induces CD4 and CD8 T cell expansion, cytokine production, and the development of cytolytic effector function. J. Immunol. *168*, 4897–4906.

Wiest, D.L., Ashe, J.M., Abe, R., Bolen, J.B., and Singer, A. (1996). TCR activation of ZAP70 is impaired in CD4+CD8+ thymocytes as a consequence of intrathymic interactions that diminish available p56lck. Immunity *4*, 495–504.

Wu, C.Y., Roybal, K.T., Puchner, E.M., Onuffer, J., and Lim, W.A. (2015). Remote control of therapeutic T cells through a small molecule-gated chimeric receptor. Science *350*, aab4077.

Zhao, Z., Condomines, M., van der Stegen, S.J., Perna, F., Kloss, C.C., Gunset, G., Plotkin, J., and Sadelain, M. (2015). Structural design of engineered costimulation determines tumor rejection kinetics and persistence of CAR T cells. Cancer Cell *28*, 415–428.

Zhou, X., Di, S.A., Tey, S.K., Krance, R.A., Martinez, C., Leung, K.S., Durett, A.G., Wu, M.F., Liu, H., Leen, A.M., et al. (2014). Long-term outcome after haploidentical stem cell transplant and infusion of T cells expressing the inducible caspase 9 safety transgene. Blood *123*, 3895–3905.

STAR★METHODS

KEY RESOURCES TABLE

REAGENT or RESOURCE	SOURCE	IDENTIFIER
Antibodies		
Anti-CAR19 (clone 233-4A)	Gift from Dr. Lawrence Cooper, MD Anderson	N/A
Anti-CD3 (clone OKT3)	Miltenyi Biotec	Cat# 130-093-387; RRID: AB_1036144
Anti-CD28 (clone CD28.2)	BD Biosciences	Cat# 555725; RRID: AB_396068
Goat anti-mouse Ig-APC	BD Biosciences	Cat# 550826; RRID: AB_398465
hCD3-PE (clone SK7)	BD Biosciences	Cat# 347347; RRID: AB_400287
hCD3-APC (clone SK7)	BD Biosciences	Cat# 340440; RRID: AB_400513
hCD4-PE (clone SK3)	BD Biosciences	Cat# 347327; RRID: AB_400283
hCD8-FITC (clone SK1)	BD Biosciences	Cat# 347313; RRID: AB_400279
hCD19-PE (clone SJ25C1)	BD Biosciences	Cat# 340364; RRID: AB_400018
hCD45-FITC (clone 2D1)	BD Biosciences	Cat# 347463; RRID: AB_400306
hCD45-PE (clone HI30)	BD Biosciences	Cat# 555483; RRID: AB_395875
hCD69-FITC (clone L78)	BD Biosciences	Cat# 347823; RRID: AB_400353
hCD69-PE-Cy7 (clone FN50)	BD Biosciences	Cat# 557745; RRID: AB_396851
hPD-1-PE-Cy7 (clone EH12.1)	BD Biosciences	Cat# 561272; RRID: AB_10611585
hTIM3-BV711 (clone 7D3)	BD Biosciences	Cat# 565566; RRID: AB_2744370
Anti-CD3pY83 (clone EP7769(2)Y)	Abcam	Cat# ab68236; RRID: AB_11155460
Anti-CD3pY142 (clone EP265(2)Y)	Abcam	Cat# ab68235; RRID: AB_11156649
Anti-HA (clone C29F4)	Cell Signaling Tech	Cat# 3724; RRID: AB_1549585
Anti-FLAG (clone D6W5B)	Cell Signaling Tech	Cat# 14793; RRID: AB_2572291
Anti-ZAP70pY319	Cell Signaling Tech	Cat# 2701; RRID: AB_331600
Anti-ZAP70 (clone D1C10E)	Cell Signaling Tech	Cat# 3165; RRID: AB_2218656
Anti-LATpY191	Cell Signaling Tech	Cat# 3584; RRID: AB_2157728
Anti-LAT	Cell Signaling Tech	Cat# 9166; RRID: AB_2283298
Anti-LCK (clone L22B1)	Cell Signaling Tech	Cat# 2657; RRID: AB_2136314
Anti-LCK (clone V49, for IP)	Cell Signaling Tech	Cat# 2714; RRID: AB_836893
Anti-THEMIS	Cell Signaling Tech	Cat# 4482; RRID: AB_11217437
Anti-SHP1 (clone C14H6)	Cell Signaling Tech	Cat# 3759; RRID: AB_2173694
Anti-CD3z (clone F-3)	Santa Cruz	Cat# SC-166275; RRID: AB_2073161
Anti-FKBP (clone H-5)	Santa Cruz	Cat# SC-133067; RRID: AB_2102847
Anti-β-actin (clone C4)	Santa Cruz	Cat# SC-47778; RRID: AB_626632
Anti-CD3ζ-HRP (clone F-3)	Santa Cruz	Cat# SC-166275; RRID: AB_2073161
Anti-FLAG (clone M2)	Sigma	Cat# F1084; RRID: AB_262044
Anti-CD4-HRP (clone EPR6855)	Abcam	Cat# ab195842; RRID: AB_2819211
Anti-CD8α (clone 144B)	Abcam	Cat# ab17147; RRID: AB_443686
Biological Samples		
Buffy coats from healthy donors	Gulf Coast Regional Blood Center, Houston, TX	N/A
Fetal liver tissues	Advanced Bioscience Resources, Alameda, CA	N/A
Chemicals, Peptides, and Recombinant Proteins		
AP21967 (A/C Heterodimerizer)	Takara/Clontech	Cat# 635055
RetroNectin	Takara/Clontech	Cat# T100B
Calcium Assay Kit	BD	Cat# 640176
PP2	Sigma	Cat# P0042

(*Continued on next page*)

Continued

REAGENT or RESOURCE	SOURCE	IDENTIFIER
Lck Inhibitor II (CAS 918870-43-6)	Millipore	Cat# 428206
Human IL-7	PeproTech	Cat# 200-07
Human IL-15	PeproTech	Cat# 200-15
GeneJuice	Merck Millipore	Cat# 70967
Phusion PCR master mix	Thermo	Cat# F-531
XenoLight D-Luciferin	Perkin Elmer	Cat# 122799
Critical Commercial Assays kit		
Human IFN-gamma ELISA kit	R&D systems	Cat# DY285B
Human IL-2 ELISA kit	R&D systems	Cat# DY202
Mouse IL-6 DuoSet ELISA kit	R&D systems	Cat# DY406-05
ELISA substrate reagent pack	R&D systems	Cat# DY999
Luminex Human Magnetic Assay	R&D systems	Cat# LXSAHM
Luminex Mouse Magnetic Assay	R&D systems	Cat# LXSAMSM
Experimental Models: Cell Lines		
BV173	German Cell Culture Collection	Cat# ACC 20
Jurkat	ATCC	Cat# TIB-152
Daudi-FFLuc	This lab (Vera et al., 2006)	PMID: 16926291
Raji-FFluc	This lab (Hoyos et al., 2010)	PMID: 20428207
CHLA-255-FFluc	Gift from Dr. Metelitsa, Baylor College of Medicine, Houston TX	N/A
Recombinant DNA		
CAR19.28ζ	This lab (Savoldo et al., 2011)	PMID: 21540550
CAR19.BBζ	This lab (Diaconu et al., 2017)	PMID: 28187946
CAR19.28AAAζ	This manuscript	N/A
CAR19.28YFζ	This manuscript	N/A
CAR19.28AFAAζ	This manuscript	N/A
CAR19.BBζ-ΔC10	This manuscript	N/A
CAR19.28.CD3Y6Fζ	This manuscript	N/A
CAR19.BB.CD3Y6Fζ	This manuscript	N/A
CAR.CD8h.CD28TM.28ζ	This manuscript	N/A
CAR.CD8h.CD28TM.BBζ	This manuscript	N/A
CAR.IgG1h.CD8TM.28ζ	This manuscript	N/A
CAR.IgG1h.CD8TM.BBζ	This manuscript	N/A
CARGD2	This lab (Chen et al., 2019)	PMID: 30617136
CAR138	This lab (Sun et al., 2019)	PMID: 31040928
PM-FRB-mRFP-T2A-FKBP-5-ptase	Addgene	Cat# 40896
FKBP-SHP1	This manuscript	N/A
CAR19.28ζ.FRB.FLAG	This manuscript	N/A
SFG.THEMIS	This manuscript	N/A
SFG.LCK	This manuscript	N/A
SFG.CD8α-SKS	This manuscript	N/A
SFG.CD8α-WT	This manuscript	N/A
SFG.CD4	This manuscript	N/A
Oligonucleotides		
THEMIS shRNA #1: 5'-GAGATCACTGAAGAGCAATAT-3'	UNC shRNA Core Lab	TRCN0000128476
THEMIS shRNA #2: 5'-CCCATAGTGACTGAAGTCATA-3'	UNC shRNA Core Lab	TRCN0000130264
SHP1 shRNA #1: 5'-GCATGACACAACCGAATACAA-3'	UNC shRNA Core Lab	TRCN0000006886
SHP1 shRNA #2: 5'-CGACATGCTCATGGAGAACAT-3'	UNC shRNA Core Lab	TRCN0000006887

(*Continued on next page*)

Continued

REAGENT or RESOURCE	SOURCE	IDENTIFIER
Software and Algorithms		
Flowjo v10	FlowJo, LLC	N/A
GraphPad Prism	GraphPad Software Inc.	N/A
Living Image v4.5.2 (IVIS imaging)	Perkin Elmer	N/A
Other		
Counting beads	Invitrogen	Cat# C36950

LEAD CONTACT AND MATERIALS AVAILABILITY

Plasmids generated in this study will be made available on request, but we may require a payment and/or a completed Materials Transfer Agreement if there is potential for commercial application. Further information and requests for resources and reagents should be directed to and will be fulfilled by the Lead Contact, Gianpietro Dotti (gdotti@med.unc.edu).

EXPERIMENTAL MODEL AND SUBJECT DETAILS

Cell Lines and Cell Culture

293T cells were cultured in IMDM (Gibco, Invitrogen) supplemented with 10% fetal bovine serum (FBS, HyClone, Thermo Scientific), 2 mM GlutaMax, 100 I.U./mL penicillin and 100 μg/mL streptomycin (Invitrogen). BV173, Jurkat, Daudi-FFLuc, Raji-FFluc, and CHLA-255-FFluc cell lines were cultured in RPMI-1640 (Gibco, Invitrogen) supplemented with 10% FBS (HyClone), 2 mM GlutaMax, 100 I.U./mL Penicillin and 100 μg/mL Streptomycin (Invitrogen). All cell lines were routinely tested for mycoplasma.

Human Samples

For the humanized mouse construction, human fetal liver tissues were obtained from elective or medically indicated termination of pregnancy through a non-profit intermediary working with outpatient clinics (Advanced Bioscience Resources, Alameda, CA). The use of the tissue in research had no influence on the decision regarding termination of the pregnancy. Informed consent of the maternal donor is obtained in all cases, under regulation governing the clinic. We were provided with no information regarding the identity of the patients, nor is this information traceable. The project was reviewed by Office of Human Research Ethics at the University of North Carolina at Chapel Hill, which has determined that this submission does not constitute human subjects research as defined under federal regulations [45 CFR 46.102 (d or f) and 21 CFR 56.102(c)(e)(l)] and does not require IRB approval.

Mouse Studies

Male and female NSG (NOD-scid IL2Rg^{null}) mice were purchased from the Animal Core Facility at UNC. Female SCID-beige (C.B-*Igh*-1b/GbmsTac-*Prkdc*^{scid}-*Lyst*^{bg}N7) mice were purchased from Taconic Biosciences. All the mice were housed in the Animal Core Facility at UNC. All mouse experiments were performed in accordance with UNC Animal Husbandry and Institutional Animal Care and Use Committee (IACUC) guidelines and were approved by UNC IACUC. For the humanized mouse model to evaluate the effects of SHP1 heterodimerization in CAR-T cells *in vivo*, humanized NSG mice (NSG-hu HSC) were generated as previously reported (Li et al., 2014). Briefly, human fetal liver tissues were obtained from elective or medically indicated termination of pregnancy through a non-profit intermediary working with outpatient clinics (Advanced Bioscience Resources). CD34^{+} hematopoietic stem cells (HSC) were transplanted in newborn NSG mice through intra-liver injection of 2 × 10^{5} purified HSC. Human immune cell engraftment was detected by flow cytometry 12 weeks after transplantation. This model reconstitutes high amount of normal human B cells that can be targeted by CD19-specific CAR-T cells, which causes the release of human IL-6 in the plasma of the treated mice.

METHOD DETAILS

Plasmids

CD19-specific CARs were constructed using the scFv from the FMC63 monoclonal antibody (Ab) the CD8α stalk including hinge and transmembrane domain and CD3ζ chain intracytoplasmic domain (Diaconu et al., 2017). CAR19.28ζ and CAR19.BBζ contained CD28 and 4-1BB endoplasmic domains, respectively. CAR19.28AAAζ (mutation of PYAPP to AYAAA), CAR19.28YFζ (mutation of PYAPP to PFAPP), CAR19.28AFAAζ (mutation of PYAPP to AFAAA) and CAR19.BBζ-ΔC10 were generated by overlapping PCR. CARGD2 (targeting the GD2 antigen) and CAR138 (targeting the CD138 antigen) were generated by replacing the scFv of CAR19. CARs with the IgG1 hinge or the CD28 transmembrane domain were cloned by overlapping PCR to replace CD8α hinge or transmembrane domain. CAR19.28.CD3Y6Fζ and CAR19.BB.CD3Y6Fζ were generated by gene synthesis (GeneArt, Thermo Scientific) and cloned into the original CAR19.28ζ construct. The full-length human THEMIS (GenBank:

NM_001164685.1) and LCK (GenBank: NM_001042771.2) were PCR amplified from a cDNA library of activated T cells, and cloned into the SFG retroviral vector after the addition of the HA or FLAG tags. Gene expression was verified in both 293T and T cells by western blot. FRB and FKBP domains were cloned by PCR from plasmid PM-FRB-mRFP-T2A-FKBP-5-ptase (Addgene #40896). SHP1 full length (GenBank: NM_002831.5) was PCR amplified from a T cell cDNA library, and cloned into the SFG vector with FKBP. CAR19.28ζ.FRB.FLAG was generated by overlapping PCR. Lentiviral constructs encoding shRNAs were obtained from UNC shRNA Core Lab and tested for knockdown efficiency in primary T cells. Two functional shRNAs were selected for functional assays.

Retrovirus and Lentivirus Production

Retroviral supernatants were prepared as previously described (Vera et al., 2006). Briefly, 293T cells were transfected with 3 plasmids (retroviral transfer vector, Peg-Pam-e encoding gag-pol, and RDF encoding the RD114 envelope), using GeneJuice transfection reagent (Novagen). Supernatants were collected at 48 and 72 hr. Lentiviral supernatants were produced in 293T cells with 3 different plasmids (lentiviral transfer vector, ps.pAX2 for lentiviral gag-pol and pMD.2G for VSV-G envelope). Supernatant was collected at 48 hr for transduction of T cells.

Transduction and Expansion of Human T Cells

Buffy coats from healthy donors were obtained through the Gulf Coast Regional Blood Center, Houston, TX. Peripheral blood mononuclear cells (PBMCs) were isolated with Lymphoprep density separation (Fresenius Kabi Norge) and activated using 1 μg/mL α-CD3 (Miltenyi Biotec) and 1 μg/mL α-CD28 (BD Biosciences) mAb coated plates. Forty eight hr later, T lymphocytes were transduced with retroviral or lentiviral supernatants using retronectin-coated plates (Takara Bio), and expanded in complete medium (45% RPMI-1640 and 45% Click's medium (Irvine Scientific), 10% FBS (Hyclone), 2mM GlutaMAX, 100 I.U./mL of Penicillin and 100 μg/mL of Streptomycin) with IL-7 (10 ng/mL; PeproTech) and IL-15 (5 ng/mL; PeproTech) or IL-2 (50 U/ml; R&D) (Zhou et al., 2014). Four to seven days later, cells were collected for *in vitro* or *in vivo* experiments. Lentiviral transduced cells were selected in 1 μg/ml puromycin (Sigma) for 3 - 5 days before T cells were used in functional assays.

Flow Cytometry and Cell Phenotyping

CAR19 expression on T cells was detected with CAR19 α-idiotype antibody followed by a goat α-mouse APC secondary Ab (BD bioscience) (Diaconu et al., 2017). Murine α-human CD3, CD4, CD8, CD45, CD69 and CD19 Abs were obtained from BD Bioscience. Samples were acquired on a Canto II or Fortessa flow cytometer from BD and data were analyzed using the FlowJo software (Tree star).

Activation of CD19-Specific CAR-T Cells with the Anti-idiotype Ab or $CD19^+$ Tumor Cells

α-CAR19 and α-CD3 Abs were serially diluted 2-fold, and coated on non-tissue culture treated 96-well plates for 16 hr. Plates were washed twice before plating T cells (2.5×10^5 cells/well). Plates were centrifuged at 1,000g for 5 min, and incubated at 37°C for 6 hr. Plates were then briefly spun, and 200 μl of the supernatant was collected for ELISA. Cells were collected and stained with α-CAR19, CD4-PE, CD69-FITC Abs and Zombie Aqua™ dye (Biolegend) at 4°C for 30 min. Samples were fixed and stored for flow cytometry analysis. For tumor cell-mediated activation, 5×10^4 BV173 tumor cells were seeded in each well of 96-well plates, and T cells were serially diluted and seeded. Six hr later, supernatant was collected for ELISA.

Cytokine Measurements

Cytokines in culture supernatants and plasma were measured using enzyme-linked immunosorbent assay (ELISA) or magnetic luminex assay following manufacturer's instructions (R&D Systems). Data were collected and analyzed using the Lumina-200 System and the Bio-Plex Manager 6.1 software (Bio-Rad).

Ca^{2+} Influx Assay

T cells were incubated with Ca^{2+} indicator as per manufacturer's instructions (Ca^{2+} influx assay, BD Bioscience). Cells were incubated with α-CAR19 Ab followed by goat α-mouse secondary Ab on ice. Ca^{2+} current was measured by flow cytometry for time-lapsed fluorescence change. Cells were first collected on ice as the baseline of the Ca^{2+} current, and then activated at 37°C for the Ca^{2+} current during T cell activation.

Immunoprecipitation (IP)

Proteins from T cells were extracted in RIPA lysis buffer (Thermo Scientific) supplemented with 1 x protease/phosphatase Inhibitors (Thermo Scientific). Equal amount of total proteins was used for IP. Rabbit/mouse IgG (Thermo Scientific) with protein G magnetic beads (Bio-Rad) was used to pre-clear the lysate and α-CAR19, α-HA or α-FLAG Abs were incubated with lysate for 16 hr, and protein G beads were then used for the pull-down. IP products were dissolved in 2 x SDS Laemmli buffer for Western blot analysis. For mass spectrometry, $>5 \times 10^8$ T cells were lysed and α-CAR19 Ab was first crosslinked on protein G beads with Dimethyl pimelimidate (DMP, Thermo Scientific). 2 x SDS Laemmli buffer without β-mercaptoethanol was used to dissolve the IP product, and β-mercaptoethanol was supplemented before western blot.

Western Blot

Protein lysate was normalized according to the amount of CAR expression and resolved on 4% - 15% SDS polyacrylamide gel electrophoresis gels (SDS-PAGE, Bio-Rad). After protein transfer onto Polyvinylidene fluoride membranes (Bio-Rad), membranes were blocked in 5% non-fat milk in TBS-T and incubated with primary and secondary Abs in TBS-T with 1% milk. The following Abs were used: α-CD3pY83 and α-CD3pY142 (Abcam), α-ZAP70pY319, α-ZAP70, α-LATpY191, α-LAT, α-LCK, α-THEMIS, α-SHP1 and α-HA tag (Cell Signaling Technology), α-CD3ζ, α-FKBP, α-β-actin (Santa Cruz), α-FLAG (M2) (Sigma) and horseradish peroxidase conjugated secondary Abs (Goat-α-mouse, Goat-α-Rabbit from Thermo Scientific). Membranes were developed with with SuperSignal West Femto Maximum Sensitivity Substrate (Thermo Scientific) on a Gel station (Bio-Rad).

Mass Spectrometry

Immunoprecipitated samples (3 biological replicates) were subjected to SDS-PAGE and stained with coomassie. Lanes for each sample were excised and the proteins were reduced, alkylated, and in-gel digested with trypsin overnight at 37°C. Peptides were extracted, desalted with C18 spin columns (Pierce) and dried via vacuum centrifugation. Peptide samples were stored at −80°C until further analysis. The peptide samples were analyzed by liquid chromatography coupled to tandem mass spectrometry (LC-MS/MS) in 3 separated experiments using a Thermo Easy nLC 1000 coupled to a QExactive HF or a Waters nanoAcquity coupled to a Thermo LTQ-Orbitrap Velos. Samples were injected onto a PepMap C18 column (75 μm id × 25 cm, 2 μm particle size) (Thermo Scientific) and separated over a 90 or 120 min gradient where mobile phase A was 0.1% formic acid in water and mobile phase B consisted of 0.1% formic acid in ACN. The LTQ-Orbitrap Velos was operated in data-dependent mode where the 10 most abundant precursors were selected for CID fragmentation (35% CE). The QExactive HF was operated in data-dependent mode where the 15 most intense precursors were selected for subsequent HCD fragmentation (27 NCE). For the second replicate, a targeted analysis of THEMIS peptides was conducted. The QExactive HF was operated in PRM mode, and an inclusion list was used to target previously identified THEMIS peptides. Raw data files were processed using Proteome Discoverer version 2.1 (Thermo Scientific). Peak lists were searched against a reviewed Uniprot human database and appended with the CAR-T sequences using Sequest. The following parameters were used to identify tryptic peptides for protein identification: 10 ppm precursor ion mass tolerance; 0.02 Da product ion mass tolerance for QE HF data and 0.6 Da for Velos data; up to two missed trypsin cleavage sites; carbamidomethylation of Cys was set as a fixed modification; oxidation of Met, acetylation of N-terminus and phosphorylation of Ser, Thr and Tyr were set as variable modifications. The ptmRS node was used to localize the sites of phosphorylation. Peptide false discovery rates (FDR) were calculated by the Percolator node using a decoy database search and data were filtered using a 5% FDR cutoff.

Xenograft Mouse Models

For long-term *in vivo* cytotoxicity, male or female NSG (NOD-scid IL2Rg^{null}) mice were injected intravenously (i.v.) with 2 x 10^6 CD19$^+$ Daudi tumor cell line labeled with the Firefly luciferase gene (Daudi-FFLuc). Four to seven days later, mice received T cells control or expressing CARs intravenously (i.v.). For tumor re-challenging experiments, 2 x 10^6 CD19$^+$ Daudi-FFLuc cells were i.v. injected at indicated time point. Tumor growth was monitored every 2 - 3 days by injecting mice intraperitoneally (i.p.) with D-luciferin (150 mg/kg, Xenolight, PerkinElmer). Photon emission was analyzed using the Xenogen-IVIS Imaging System as previously validated (Diaconu et al., 2017). For short-term *in vivo* T cell activation, NSG mice were injected with Daudi-FFLuc cells i.v. Two weeks later, CAR19.28ζ-Ts were labeled with Cell-trace Violet (Thermo Scientific) and CAR19.BBζ-Ts were labeled with CFSE (Thermo Scientific) as per manufacturer's instructions. Cells were mixed 1:1, and a total 1 x 10^7 cells were i.v. injected in each mouse. Peripheral blood, bone marrow, lung and spleen were harvested 6 hr after T cell injection, dissociated into single cells and stained with α-human CD45-PE, CD3-APC and CD69-PE-Cy7 Abs. For the neuroblastoma metastatic model, 6 - 8-week-old male or female NSG mice were injected i.v. with CHLA-255-FFluc tumor cell line (2 × 10^6 cells/mouse). Fourteen days after tumor inoculation, CAR-T cells were infused i.v. (Chen et al., 2019). For the NSG mouse model to evaluate the effects of SHP1 heterodimerization in CAR-T cells *in vivo*, mice were injected i.v. with 2 x 10^6 Daudi-FFLuc cells. Seven days later, 2 x 10^6 T cells were infused i.v.. AP21967 was administrated intraperitoneally twice at 10 mg/kg dose. Tumor growth was monitored twice a week.

Cytokine Release Syndrome Models

Evaluation of CRS in humanized NSG mice was performed as previously described (Diaconu et al., 2017). Mice were infused with 5 x 10^6 CAR-T cells at day 0, and plasma was collected at days 1 and 2. AP21967 was administrated intraperitoneally at 10 mg/kg dose (Rivera et al., 2012). Weight of each mouse was normalized to starting weight before CAR-T cell infusion. In a second CRS murine model, 7 - 10-week-old female SCID-beige (C.B-*Igh*-1b/GbmsTac-*Prkdc*^{scid}-*Lyst*^{bg}N7, Taconic Biosciences) mice were injected i.p. with Raji-FFluc cells (Giavridis et al., 2018). After 21 days, mice were grouped based on the BLI (total flux). Mice were infused i.p. with 30 x 10^6 CAR-T cells. Weight of each mouse was normalized to starting weight before CAR-T cell infusion.

Co-culture Assays

CD19$^+$ BV173 tumor cells were seeded into 24-well plates with 5 x 10^5 cells/well and T cells were added at different effector to target (E:T) ratios (E:T=1:1 or 1:5). After 24 hr, supernatant was collected for ELISA. Three days later, cells were collected and stained with α-human CD3 and CD19 Abs for flow cytometry analysis.

Immunofluorescence and Confocal Microscopy

Ctrl and CAR19.BBζ-T cells with or without FLAG-tagged LCK at day 6 of culture were first stained with CAR19 α-idiotype Ab followed by the goat anti-mouse IgG conjugated with AlexaFluor 647 (Invitrogen) secondary Ab to detect CAR19 expression. Cells were then fixed and permeabilized with Cytofix/Cytoperm solution (BD Bioscience) according to manufacturer's instructions. Intracellular FLAG-tagged LCK was detected with Rabbit α-FLAG (Cell Signaling Technology) and goat anti-Rabbit IgG conjugated with AlexaFluor 488 (Invitrogen). Cells were then loaded on slides by Cytospin Cytocentrifuge (Thermo Scientific) and mounted with ProLong Diamond Antifade Mountant with DAPI (Thermo Scientific). Slides were imaged using confocal microscopy (Zeiss LSM710) and images were analyzed with Fiji software (ImageJ).

QUANTIFICATION AND STATISTICAL ANALYSIS

Data were presented as mean ± SEM unless indicated otherwise. Statistical analyses were performed using GraphPad Prism software. Two-tailed unpaired *t*-test, one-way ANOVA, and two-way ANOVA were used. Bonferroni's correction for multiple comparisons was used to calculate adjusted p value when appropriate. The exact p values were shown in figures; *ns*, not significant. Specific statistical test used for each figure was described in the corresponding figure legend.

DATA AND CODE AVAILABILITY

This study did not generate datasets.